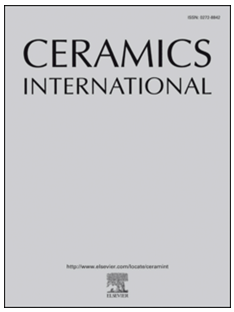

Thermoelectric modules built using ceramic legs grown by laser floating zone

N.M. Ferreira, D. Lopes, A.V. Kovalevsky, F.M. Costa, A. Sotelo, M.A. Madre, A. Rezania

PII: S0272-8842(20)31873-3

DOI: https://doi.org/10.1016/j.ceramint.2020.06.213

Reference: CERI 25640

To appear in: *Ceramics International*

Received Date: 27 February 2020

Revised Date: 17 May 2020

Accepted Date: 18 June 2020

Please cite this article as: N.M. Ferreira, D. Lopes, A.V. Kovalevsky, F.M. Costa, A. Sotelo, M.A. Madre, A. Rezania, Thermoelectric modules built using ceramic legs grown by laser floating zone, *Ceramics International* (2020), doi: https://doi.org/10.1016/j.ceramint.2020.06.213.

Thermoelectric Modules Built Using Ceramic Legs Grown by Laser Floating Zone

N.M. Ferreira[1,*], D. Lopes[2], A.V. Kovalevsky[2], F.M. Costa[1], A. Sotelo[3], M. A. Madre[3], A. Rezania[4]

1- i3N, Physics Department, University of Aveiro, Aveiro, Portugal
2- CICECO - Aveiro Institute of Materials, Department of Materials and Ceramic Engineering, University of Aveiro, Aveiro, Portugal
3- ICMA, CSIC-Universidad de Zaragoza, Zaragoza, Spain
4- Department of Energy Technology, Aalborg University, Pontoppidanstræde 111, 9220 Aalborg, Denmark

* - nmferreira@ua.pt

Abstract

The present work reports the first attempt of thermoelectric module design, based on oxide materials grown through the laser floating zone technique. Two modules with 4-legs thermoelectric were assembled using $Bi_2Ba_2Co_2O_y$ fibres as p-type legs, while $Ca_{0.9}La_{0.1}MnO_3$ and $CaMn_{0.95}Nb_{0.05}O_3$ fibres were used as n-type legs. Structural and electrical characterisation of the individual fibres was performed, and the results compared to the literature. The evolution of open-circuit voltage on heating and cooling in the range up to 723 K, present the expected trends based on the Seebeck coefficient of the individual fibres, suggesting good reliability of the modules during temperature cycling. The power generation performance was evaluated for a temperature difference up to 500 K under different electric loads. The maximum measured power was ~2.2 mW for a module volume of ~ 39 mm^3. Nevertheless, the module here studies possess better performance than those commercially available.

Keywords

Thermoelectric module, laser floating zone, thermoelectric oxide, thermoelectric performance, n- and p-type Thermoelectric materials

1. Introduction

Thermoelectric materials present a unique power generation solution due to their capability to transform waste thermal energy into electricity without requiring moving components. Thermoelectric generators (TEG) are solid-state devices formed by the combination of different units, or legs/thermoelements. These legs involve n- and p-type semiconducting materials which have to be electrically connected in series and thermally in parallel. The advancements that have been made for these thermoelectric materials were mostly focused on their energy conversion efficiency envisaging their commercial production. To materialize their potential and, at the same time, improve TEG efficiency, the gap between thermoelectric materials development and generator systems design and engineering must be closed [1].

Several methods for measuring the power-generation performance of thermoelectric modules are described in the literature [1-6]. Moreover, some of them are applied to specific fields such as industrial furnaces, automobile, solar thermal energy systems, and so on, as they have been actively promoted by private companies. The durability and efficiency of TEG systems in practical fields is the key to success at the next stage [3, 7, 8]. It is well-known that the characteristics of electronic and thermal transport in the legs are decisive for the overall system performance [3-8].

Skomedal et al. [9] presented the relationship between the characteristics of each leg of the TEG and the final parameters of the module, such as the internal resistance, open-circuit voltage, and maximum generated power. It is known that the figure of merit $ZT= S^2\sigma T/k$ is used to describe the performances of each TE material, depending on the properties: Seebeck coefficient (S), electrical conductivity (σ), thermal conductivity (k), and absolute temperature (T) [9].

The typical materials used in current commercial modules (Bi_2Te_3, PbTe, SiGe, etc.) usually contain toxic, expensive, heavy, and scarce elements. Moreover, most of them are limited to relatively low working temperatures due to decomposition, oxidation or sublimation, when working under air. On the other hand, oxide-based thermoelectric materials are capable of operating at high temperatures under air, maintaining their structural and electric stability. However, these materials have received much less attention than the current ones, due to their relatively low efficiency [9]. Another important issue deals with the difficulties in providing reliable electrical contacts between oxide-based legs and interconnecting metal stripes. For these reasons, some research groups are developing and improving thermoelectric materials and generators based on cheap and abundant oxide materials such as $Bi_2Ba_2Co_2O_x$ [10], $Bi_2AE_2Co_2O_x$ with AE = Ca, Sr, and Ba [11], $Ca_{2.7}Bi_{0.3}Co_4O_9$ and $CaMn_{0.95}Ta_{0.05}O_3$ [12], $CaMnO_3$–based materials [13] and $CaMnO_3$ and $Ca_3Co_4O_9$ [9]. Several examples of oxide-based thermoelectric modules can be found in the literature, such as: $CaMnO_3$ - $Ca_3Co_4O_9$ [9], $Ca_{2.7}Bi_{0.3}Co_4O_9$ - $CaMn_{0.95}Ta_{0.05}O_3$ [12], Li-doped NiO - $Ba_{0.2}Sr_{0.8}PbO_3$ [14], $Ca_{2.75}Gd_{0.25}Co_4O_9$ - $Ca_{0.92}La_{0.08}MnO_3$ [15],

$Ca_{2.7}Bi_{0.3}Co_4O_9$ - $CaMn_{0.98}Mo_{0.02}O_3$ [16], $Ca_{2.7}Bi_{0.3}Co_4O_9$ - $La_{0.9}Bi_{0.1}NiO_3$ [17, 18], $Ca_3Co_4O_9$ - $(ZnO)_7In_2O_3$ [19] and Bi_2Te_3 – CMO [20]. Most of them were assembled using cobaltites as p-type material, while n-type one was mainly based on calcium manganites. So far, the best modules have reached 56 mW/cm^2 power density ($=P_{max}/A_{TE}$; P_{max} is maximum power, and A_{TE} is the total TE area) with 760 K temperature difference [9].

This work provides a perspective of thermoelectric generator development using materials obtained by laser processing. It represents the first attempt to generally assess the prospects for building thermoelectric generators based on the thermoelectric materials prepared by the laser floating zone technique. One of the main advantages of this technology is the possibility to produce fibre-like thermoelectric elements [21], which are suitable for assembling of the thermoelectric module, along with providing unique processing conditions for the material design. Moreover, these fibres present good thermoelectric properties, based on the results published in several works [10, 11, 13, 22-24]. Thus, the Laser Floating Zone (LFZ) technology shows excellent prospects for tailoring the thermoelectric performance, but until now nor attempts to test laser-processed thermoelements in a module configuration were reported. On the other hand, the fibres produced by the LFZ are subjected to dimensional constraints (typical diameters < 2mm). This represents a limit of normally available equipment, but not the technology itself, which is pretty scalable. Consequently, in most cases, it is not possible to measure their thermal conductivity using most of the commercial devices. Moreover, when it is possible to perform these measurements, they are limited to a maximum temperature of 473 K. For this reason, most publications dealing with fibres produced by LFZ [10, 11, 13], report only PF ($=S^2\sigma$) values. One solution could be the direct characterization of fibres in a TEG module. The underlying idea is understanding the relationships between the fibres performances and the thermoelectric generator system efficiency. Taking into account previously published works, the selected TE materials correspond to $Bi_2Ba_2Co_2O_x$ as p-type [10, 11], and $(Ca,La)MnO_3$ and $Ca(Mn,Nb)O_3$ as n-type [13]. The use of these fibres allows producing textured materials with adequate dimensions in just one processing step.

2. Experimental procedure

The selected sample preparation procedure is similar to that described elsewhere [11, 13]. Appropriate proportions of Bi_2O_3 (Aldrich, 99.9%), $BaCO_3$ (Aldrich, ≥ 99.98%), Co_3O_4 (Panreac, 99.5%), $CaCO_3$ (Merck, 99%), MnO_2 (Aldrich, 99%), La_2O_3 (Aldrich, 99.99%) and Nb_2O_5 (Aldrich, 99%) were weighed to prepare: $Bi_2Ba_2Co_2O_y$ (BBCO), $Ca_{0.9}La_{0.1}MnO_3$ (CLMO), and $CaMn_{0.95}Nb_{0.05}O_3$ (CMNO). The Nb_2O_5, MnO_2 and La_2O_3 oxides were thermally treated at 1073 K during 12h, to remove the absorbed humidity before weighing. The powders were mixed in a planetary mill during 2h, to obtain a homogeneous mixture. Polyvinyl alcohol (PVA) was then added to the powders to produce rods by cold extrusion, which were dried to be used as precursors in an LFZ system described in [13]. The growth conditions have been determined from previous works [10, 11, 13], and are summarized in table 1.

Table 1 – Characteristics of the different samples, with their growth rates.

TE type	Sample Denomination	Sample Composition	Growth rate (mm/h)
n	CMNO	$CaMn_{0.95}Nb_{0.05}O_3$	100
n	CLMO	$Ca_{0.9}La_{0.1}MnO_3$	100
p	BBCO	$Bi_2Ba_2Co_2O_y$	30

After the growing processes, dimensionally homogeneous samples with a diameter of 1.75 mm were obtained in all cases. Powder XRD patterns were determined for all as-grown fibres between 20 and 70 degrees using a Panalytical X'pert PRO3 diffractometer (CuKa1 radiation) to identify the phase composition of the samples. Microstructural observations were made on longitudinal polished sections of the samples in a Hitachi SU-70 FEG-SEM microscope equipped with a Bruker EDS system. Electrical conductivity (σ) and Seebeck coefficient (S) were simultaneously measured by the standard dc four-probe technique in an LSR-3 system (Linseis GmbH) between 323 and 923 K under He atmosphere. Furthermore, from the electrical resistivity and Seebeck coefficient data, PF has been determined to establish the TE performances of fibres. Finally, dilatometric behaviour and thermal expansion coefficient of all fibres were measured on heating (3 K/min) up to 1073 K under air atmosphere, using a vertical alumina dilatometer Linseis L75V/1250.

The process to produce the CLMO-BBCO, and CMNO-BBCO TEG modules are described in figure 1. The fibres were cut into 4 mm long pieces using a diamond wire cutting machine to produce parallel faces at both ends of the samples. AlN ceramic with a Cu layer from Curamik [25] has been used as faces of the module (top and bottom layer). Before using, the electrical contacts between the thermoelectric legs were designed on the Cu layer, and the unnecessary Cu was removed. A silver paste was used to join the legs to the upper and lower faces of the module in two steps. The silver past was dried at

room temperature and then cured at 593 K for 45 minutes. This process was performed for the upper part, and then for the lower part of the module.

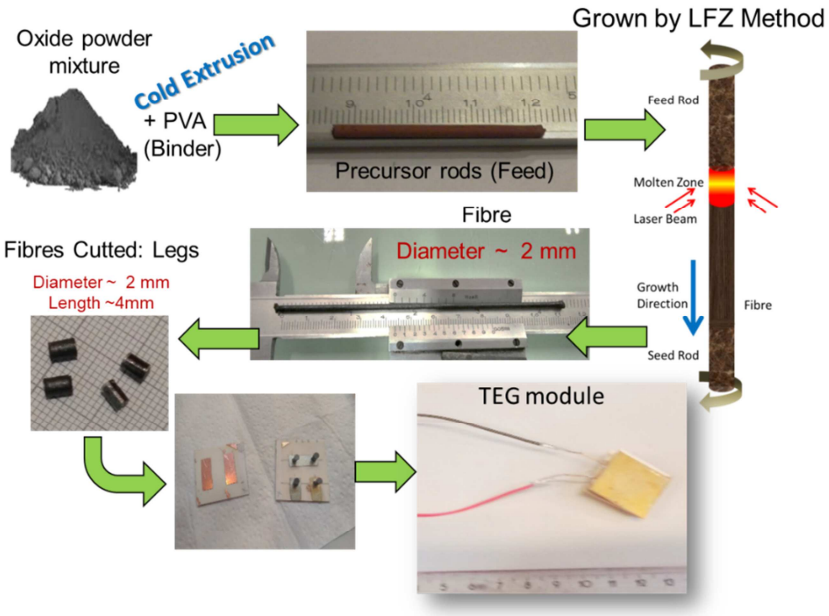

Figure 1 – Schematic steps followed to build a TEG module

Finally, the wires were connected to the module and then assembled in the TEG measurement system (figure 2) as described in [6, 26]. The measurements were performed from room temperature up to 873 K on the hot side under vacuum. The temperatures (hot and cold side) were measured by four T-type thermocouples with a diameter of 0.05 mm [6]. The cold face of the TEG has been kept between 295-323 K, depending on the hot face temperature (top face). The electric measurements were made in open circuit to determine the voltage in these conditions (V_{oc}), and in close circuit conditions to obtain the current and voltage under a load (external resistance), according to the maximum resistance of the module. All experimental data were collected by a Keysight LXI (34972A) data logger acquisition system, which allowed determining the power generated by the thermoelectric module [27]. The relative uncertainty of the equipment used was determined to be less than 2.5% [6, 28].

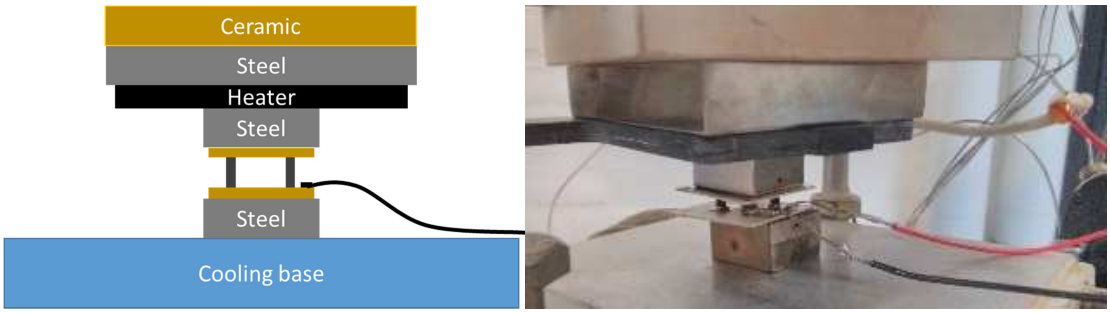

Figure 2 – Scheme of the module measuring system (left side) and a photograph of the real device (right side)

3. Results and discussion

3.1. General characterisation of the legs materials

Powder XRD patterns displayed in figure 3 show that all samples present the respective thermoelectric phase, in some cases accompanied by secondary phases, in agreement with the results of previous works [10, 11, 13, 23]. The presence of these secondary phases can be explained by the typical incongruent melting of these materials. Moreover, the samples processed by the LFZ technique in the air might be also oxygen-deficient and this could be an additional factor associated to the growth condition for the presence of the secondary phases, as reported in previous works [13, 29].

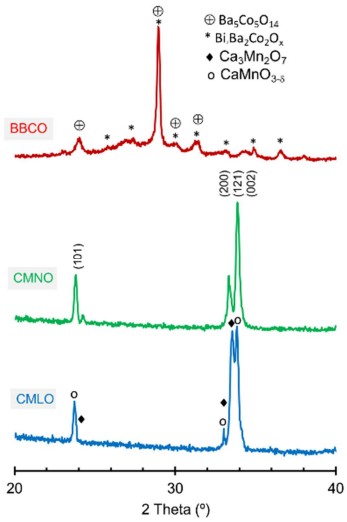

Figure 3 – Powder XRD patterns of the different as-grown materials

Microstructural SEM observations, combined with the elemental chemical distribution obtained through EDS mapping, are displayed in figure 4. As it can be observed in the figure, the representative micrographs of the fibres clearly show a more uniform distribution of the elements in the CMNO samples, indicating a lower amount of secondary phases, when compared to the other ones (CLMO and BBCO), agreed with the reported in previous works [10, 13]. Moreover, the existence of secondary phases in the fibres confirms the XRD results, previously discussed.

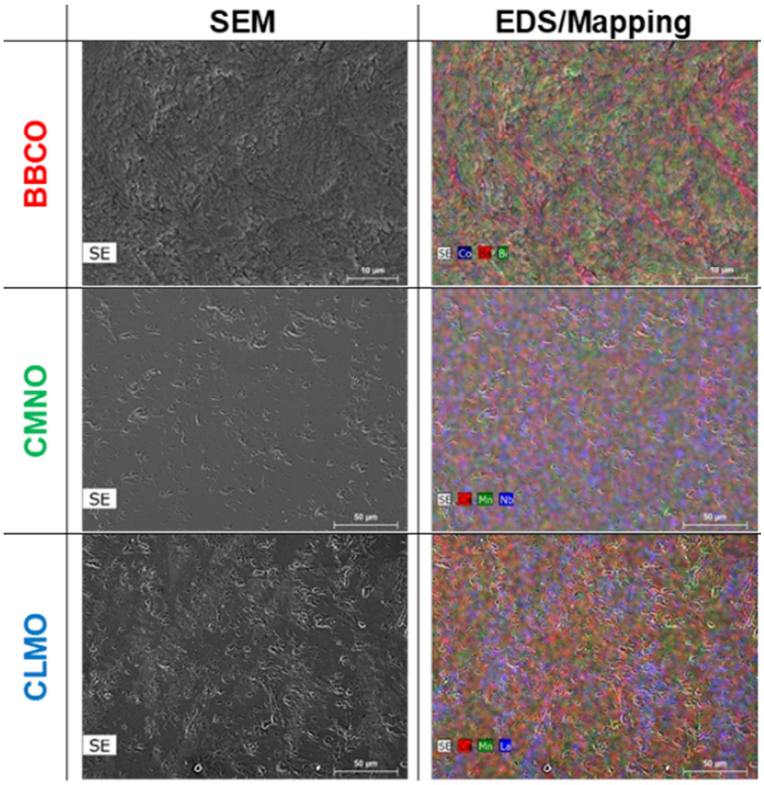

Figure 4 – Representative SEM micrographs of the longitudinal section of different samples, with the elemental mappings.

The electrical conductivity as a function of temperature for all samples is shown in figure 5a. In the graph, it can be observed that CLMO and BBCO samples present similar behaviour and values, while CMNO shows lower values in the whole measured temperature range. Moreover, all samples demonstrate semiconducting behaviour ($d\sigma/dT > 0$) in this temperature range, which is much more evident in CMNO samples. The maximum values at 923 K observed for the manganite samples (~ 10-100 S/cm) are in the same order of those obtained for similar $CaMnO_3$-based materials [30-32]. BBCO samples also present similar conductivities to the ones reported in the literature (~ 100 S/cm) for laser processed samples [10, 23], and higher than for samples prepared by solid-state route (~10 – 80 S/cm) [33, 34, 35].

Figure 5b presents the evolution of Seebeck coefficient as a function of temperature, for all samples. The graph clearly illustrates the difference between the two types of TE materials: while BBCO samples present positive values, characteristic of p-type materials (predominating hole-conduction mechanism), manganite samples display negative Seebeck coefficient values, characteristic of n-type materials (main transport charge carriers are electrons). The values obtained for this n- and p-type fibres are similar to those previously reported in the literature and explained elsewhere [10, 11, 13, 23, 33].

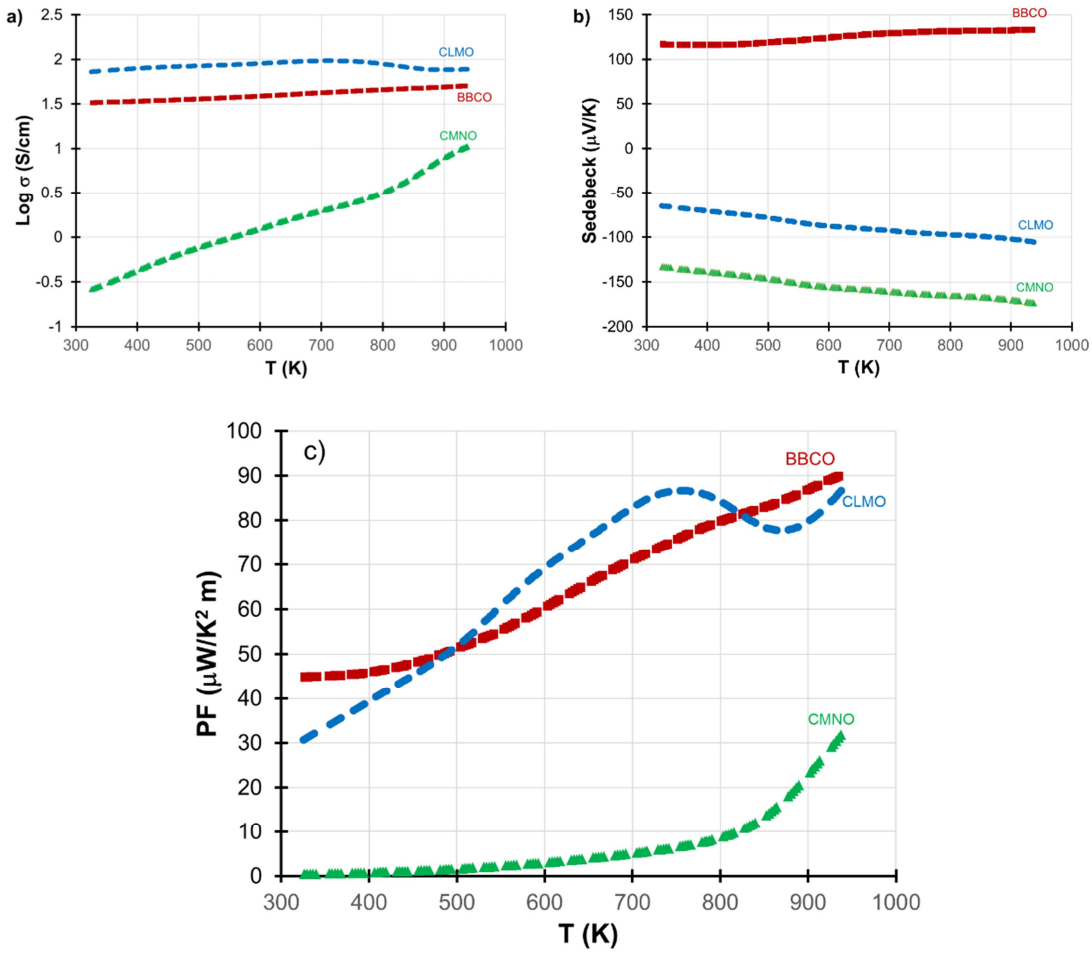

Figure 5 – Thermoelectric characterization of grown fibres: a) Electrical conductivity, b) Seebeck coefficient and c) Power Factor

Using the electrical conductivity and Seebeck coefficient data presented previously, the thermoelectric performance of all fibres can be analysed using the power factor, the corresponding data are represented in figure 5c. BiBaCoO fibres have reached PF values close to 0.1 mW/K^{2}m at 923 K, which are within the reported for these grown materials [10, 11, 23], but higher than for those prepared via solid-state route [33]. On the other hand, while CLMO fibres present similar PF values to the determined in BBCO fibres, the CMNO ones possess much lower values (0.03 mW/K^{2}m at 923 K), due to their microstructural characteristics, such as the existence or not of trends in the grain orientation to the growth axis [13].

Since the thermoelectric fibres will be subjected to a thermal difference between the hot and cold side of the modules ($\Delta T = T_{hot} - T_{cold}$), the thermal expansion behaviour is crucial for the module integrity. Consequently, the thermal expansion coefficients should be as close as possible to each other to avoid differential expansions which would be reflected in internal stresses, leading to a deterioration of modules. Hence, it is necessary to know these characteristics for the thermoelectric materials. The results obtained for all thermoelectric materials are presented in figure 6, while the mean thermal expansion coefficients are displayed in table 2. As it can be observed in the graph, at

relatively low temperatures (303 − 732K) all the fibres show quite linear behaviour, with a mean thermal expansion coefficient of around 12.5-14.0 x 10^{-6}/K for the cobaltite, and manganite fibres, respectively (see table 2). At higher temperatures, the expansion curves show deviations from linearity, which may be attributed to changes in phase composition, the concentration of point defects, or the rearrangement in the sublattices, possibly combined with oxidative decomposition from Mn^{4+} to larger Mn^{3+} [34], in the manganite fibres. Moreover, the values obtained for these manganites are within the reported in the literature (9-15 x 10^{-6}/K) [33,36-38].

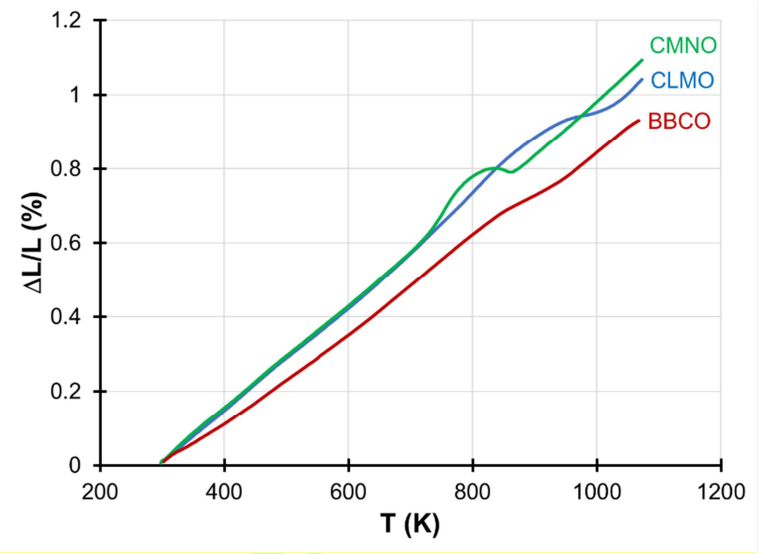

Figure 6 – Thermal expansion with the temperature of the fibres.

In the case of cobaltite fibres, they present a lower thermal expansion coefficient, when compared to the manganite ones (see figure 6 and table 2). The obtained mean thermal expansion coefficient for the BBCO fibres (12.6–13.4 x 10^{-6}/K) are slightly higher than the reported for solid-state prepared samples (9.68–13.2 x 10^{-6}/K) [33]. On the other hand, they are in the range of values reported in similar materials, which point out to the influence of composition and processing method on the mean thermal expansion coefficient values [33, 39].

Table 2 – Thermal expansion coefficient of the fibres

Sample	ΔT (K)	α ± 0.01 (10^6 K^{-1})
BBCO	423 - 723	12.58
	973 - 1073	13.44
CMNO	303 - 723	13.95
	873 - 1073	14.73
CLMO	303 - 723	13.96
	923 - 1073	14.57

3.2. Module characterisation

At the first step, the open-circuit voltage (V_{oc}) was measured for both CLMO-BBCO and CMNO-BBCO modules on heating (figure 7) to determine their behaviour with temperature. Moreover, the CLMO-BBCO module was also characterized during cooling to observe if any voltage changes occur due to decomposition or oxidation of materials. The results show similar V_{oc} values during heating and cooling cycles, illustrating the stability of these materials. This result agrees with dilatometry analysis since no change of the thermal expansion coefficient is observed below 723 K for these fibres, which might indicate the presence of oxygen exchange with the atmosphere and the corresponding impact on the electronic defects (figure 6 and table 2). However, more tests should be performed in future work to confirm the stability of the modules and reversibility of V_{oc} during heating and cooling cycles at higher temperatures. The results presented in figure 7 show a linear increase of the voltage with the difference of temperature between hot and cold sides, in both modules. Furthermore, the BBCO-CMNO module presents higher V_{oc} value (~0.16 V at ~673 K), than the BBCO-CLMO one (~0.07 V at ~ 673 K). It should be pointed out that the value of V_{oc} is similar to the sum of Seebeck coefficients (figure 5b) of BBCO-CLMO fibres and BBCO-CMNO fibres in each module [9].

Based on these results, the performances of the BBCO-CMNO module have been determined under different loads to determine the maximum generated power. During heating, the internal resistance of (both) modules changes from 10 Ω at room temperature to ~1kΩ at 623 K. Consequently, the external load resistances have been ranging between these values (6-1kΩ). However, it should be noticed that the high electrical resistance of the module is much higher than the obtained considering the resistivity of each fibre 0.01 – 0.1 Ω.cm (figure 5a). This effect can be attributed to the resistivity of the electrical contact [9], or to the distance between the legs, which should be optimized in the future modules.

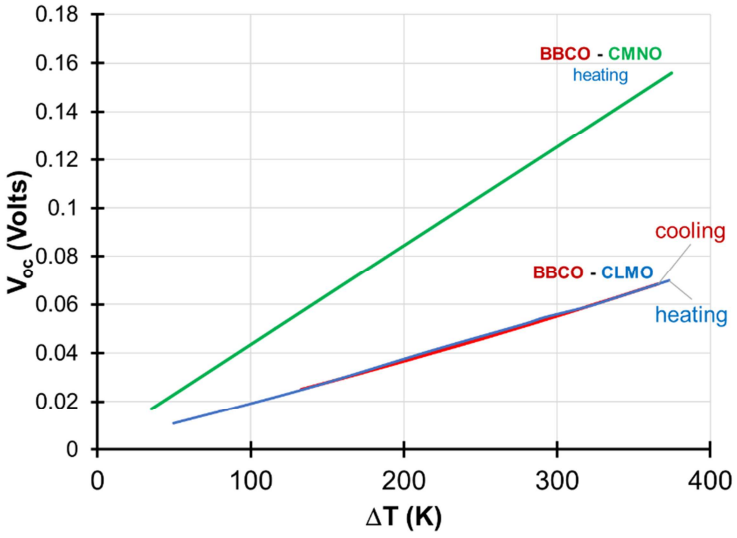

Figure 7 – Results of V_{oc} (voltage open-circuit) during heating up to a temperature difference of 450K for both modules, and also during cooling for the BiBaCoO – CaLaMnO module.

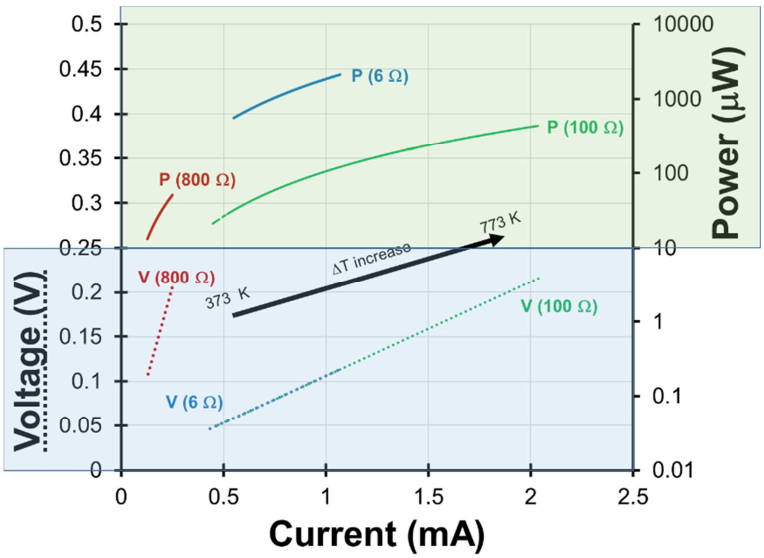

Figure 8 –V-P-I curves obtained in the BBCO – CMNO module under different loads 6, 100 and 800 Ω. Dotted lines correspond to the V-I, while continuous lines to P-I.

Corresponding results for BBCO-CMNO module measured at different temperatures and load resistances are presented in the V-P-I graph in figure 8. As it can be observed in the figure, the voltage shows a nearly linear increase with the current and decreases when the load is higher. The same behaviour is observed for the evolution of the generated power, reaching the highest power for the 6 Ω loads. On the other hand, when observing the behaviour and obtained values when using an 800 Ω load, it is clear that it is too high for the tested module.

Another consideration which can be extracted from this graph is that it is slightly different of those reported in the literature [9,12] because the behaviour of the module has been performed as a function of temperature with each load, while in these works the measurements were performed as a function of the load at each temperature. On the other hand, apart from these small differences in the graphs, the general characteristics of the measured module are similar to those reported in the literature, showing an increase of the power and current with the load up to an optimal resistance value, decreasing for higher loads.

The power generation improves with the temperature difference and when the external load is decreased, as it can be observed in figure 9, in agreement with the power equation ($P = V^2/R$). The highest temperature difference was 500K ± 3 K, achieved for 823 ± 1 K in the hot side temperature (T_h). The maximum generated power (2.21 mW) has been obtained using a 6 Ω external load under a differential temperature of 500 K.

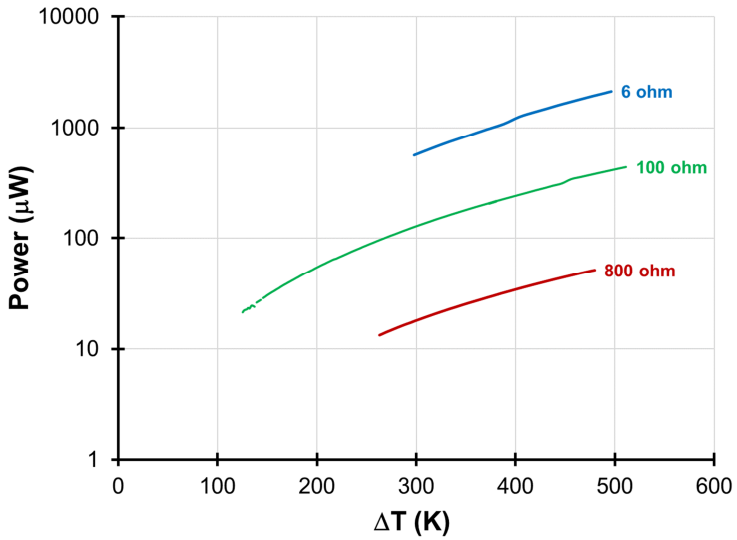

Figure 9 – Power generation evolution with the temperature difference and the external load for BBCO-CMNO module.

The characteristics of the module developed in this work can be compared with other modules reported in the literature, in table 3. In this table, some parameters, as the total volume of the module (V_{total}), maximum output power values (P_{max}) and temperature difference ($\Delta T=T_{hot}-T_{cold}$), are presented. With these parameters, $P_{max}/(V_{total}*\Delta T)$ has been calculated and presented in the last column of the table. When comparing the data, it can be observed that the module developed in this work possess an efficiency within the typical values of these oxide-based modules. On the other hand, it should be noted that modules with similar composition display a $P_{max}/(V_{total}*\Delta T)$ of 0.16 - 0.38 ($\mu W/K.mm^3$), where the reported in this work (0.113 $\mu W/K.mm^3$) is near to the best values. This difference can be associated with the external load magnitude, which can decrease the efficiency of the module (see figure 9). Consequently, further work should be performed in our modules to optimize the external load to maximize the power output. Nevertheless, it should be highlighted that the module presented in this work possess better performance than those commercially available.

Table 3 – Characteristics of modules reported in the literature.

TEG material	V_{total} (mm^3)	P_{max} (mW)	ΔT (K)	$P_{max}/(V_{total}*\Delta T)$ ($\mu W/K.mm^3$)	Ref
p: $Ca_{2.7}Bi_{0.3}Co_4O_9$ n: $CaMn_{0.98}Mo_{0.02}O_3$	900	340	975	0.3874	16
p: $Ca_{2.7}Bi_{0.3}Co_4O_9$ n: $La_{0.9}Bi_{0.1}NiO_3$	1183	150	551	0.2301	17
p: Ca_3Co_4O n: $Ca_{0.931}MnO_3$	118	15.6	800	0.1647	9
p: $Bi_2Ba_2Co_2O$ n: $CaMn_{0.95}Nb_{0.05}O_3$	39	2.21	500	0.113	Present work
p: Li-doped NiO n: $Ba_{0.2}Sr_{0.8}PbO_3$	960	34.4	539	0.0664	14
p: $Ca_{2.75}Gd_{0.25}Co_4O_9$ n: $Ca_{0.92}La_{0.08}MnO_3$	3960	63.5	390	0.0411	15
Commercial Bi–Te based TEGs	15680	30	52	0.0367	40
p: $Ca_{2.7}Bi_{0.3}Co_4O_9$ n: $CaMn_{0.95}Ta_{0.05}O_3$	12056	138	514	0.0222	12
p: $La_{1.97}Sr_{0.03}CuO_4$ n: $Nd_{1.97}Ce_{0.03}CuO_4$	8280	26.3	360	0.0088	18
p: $Ca_3Co_4O_9$ n: $(ZnO)_7In_2O_3$	445500	423	763	0.0012	19
p: Bi_2Te_3 n: CMO	35701	3.75	500	0.0002	20

Taking into account these results, further work on the optimization of distances between legs, as well as modules height, should be performed to maximize the power output of this kind of modules. Moreover, improving the characteristics of the fibres could also be considered to increase their thermoelectric efficiency.

Conclusions

In this study, a test set-up has been designed, constructed and used to investigate TEGs based on BiBaCoO (BBCO) as a p-type leg, and CaLaMnO (CLMO), or CaMnNbO (CMNO) as an n-type leg. Two thermoelectric modules combining these legs were successfully developed and tested. A maximum power output of 2.21 mW was achieved for the BBCO-CMNO module under a temperature difference of 500 K. The efficiency calculated for this module evidences the great potential of such approach, as compared to other considered modules from the literature. However, the relatively low power density obtained indicates the necessity of improving the design following the directions: (1) using the fibres after heat treatment, since their thermoelectric efficiency is improved; (2) testing other laser-grown materials as n- and p-type elements to obtain a higher thermoelectric efficiency; and (3) optimization of module fabrication to assess the optimal length, number of legs, area ratio, and improving the electrical contact.

Conflict of Interest:

No conflict of interest to declare.

Acknowledgements

The authors gratefully acknowledge the support of i3N (UIDB/50025/2020 & UIDP/50025/2020), CICECO - Aveiro Institute of Materials (UID/CTM/50011/2020) and the REMOTE project (POCI-01-0145-FEDER-031875), financed by COMPETE 2020 Program and National Funds through the FCT/MEC and when appropriate co-financed by FEDER under the PT2020 Partnership Agreement. This work was also funded by national funds (OE), through FCT – Fundação para a Ciência e a Tecnologia, I.P., in the scope of the framework contract foreseen in the numbers 4, 5 and 6 of the article 23, of the Decree-Law 57/2016, of August 29, changed by Law 57/2017, of July 19.

NM Ferreira also acknowledges the grant support from ECIU Research Mobility Fund 2019 edition that allows the visit to Aalborg University to conduct the present study.

A. Sotelo and M. A. Madre acknowledge MINECO-FEDER (MAT2017-82183-C3-1-R) and Gobierno de Aragón-FEDER (Research Group T54-17R) for financial support.

References

[1] – S. LeBlanc, Thermoelectric generators: Linking material properties and systems engineering for waste heat recovery applications, Sustainable Materials and Technologies 1–2 (2014) 26–35, DOI: 10.1016/j.susmat.2014.11.002.

[2] - B. Ciylan, S. Yılmaz, Design of a thermoelectric module test system using a novel test method, International Journal of Thermal Sciences 46 (2007) 717–725, DOI: 10.1016/j.ijthermalsci.2006.10.008.

[3] - T. Kajikawa, Advances in thermoelectric power generation technology in japan, Journal of Thermoelectricity 3 (2011) 5-18, www.jt.cv.ua, last OctSep2019.

[4] - J. Hejtmanek, K. Knizek, V. Svejda, P. Horna, M. Sikora, Test system for thermoelectric modules and materials, Journal of Electronic Materials, 43 (2014) 3726- 3732, DOI: 10.1007/s11664-014-3084-7.

[5] - C.L. Izidoro, O.H. Ando Junior, J.P. Carmo, L. Schaeffer, Characterization of thermoelectric generator for energy harvesting, Measurement 106 (2017) 283–290, DOI: 10.1016/j.measurement.2016.01.010.

[6] - M.K. Rad, A. Rezania, M. Omid, A. Rajabipour, L. Rosendahl, Study on material properties effect for maximization of thermoelectric power generation, Renewable Energy 138 (2019) 236-242, DOI: 10.1016/j.renene.2019.01.104.

[7] - J. Chen, K. Li, C. Liu, M. Li, Y. Lv, L. Jia, S. Jiang, Enhanced Efficiency of Thermoelectric Generator by Optimizing Mechanical and Electrical Structures, Energies 10 (2017) 1329; DOI:10.3390/en10091329.

[8] - D. Enescu, Thermoelectric Energy Harvesting: Basic Principles and Applications, in Green Energy Advances edited by Diana Enescu, Published by Intechopen February 2019, ISBN: 978-1-78984-200-5, DOI: 10.5772/intechopen.83495.

[9] - G. Skomedal, T. Vehus, N. Kanas, S. P. Singh, M.A. Einarsrud, K. Wiik, P. H. Middleton, Long term stability testing of oxide unicouple thermoelectric modules, Materials Today: Proceedings 8 (2019) 696–705

[10] G. Constantinescu, Sh. Rasekh, M.A. Torres, M.A. Madre, J.C. Diez, A. Sotelo, Enhancement of the high-temperature thermoelectric performance of Bi2Ba2Co2Ox ceramics, Scripta Materialia 68 (2013) 75-78, DOI: 10.1016/j.scriptamat.2012.09.014

[11] - J.C. Diez, S. Rasekh, M.A. Madre, M.A. Torres, A.E. Sotelo, High thermoelectric performances of Bi–AE–Co–O compounds directionally growth from the melt, Boletín de la Sociedad Española de Cerámica y Vidrio 57 (2018) 1-8, DOI: 10.1016/j.bsecv.2017.10.003

[12] - O.V. Merkulov, B.V. Politov, K.Yu. Chesnokov, A.A. Markov, I.A. Leonidov, M.V. Patrakeev, Fabrication and testing of a tubular thermoelectric module based on oxide elements, Journal of Electronic Materials 47 (2018) 2808- 2816, DOI:10.1007/s11664-018-6150-8

[13] - N.M. Ferreira, N.R. Neves, M.C. Ferro, M. A. Torres, M. A. Madre, F.M. Costa, A. Sotelo, A.V. Kovalevsky, Growth rate effects on the thermoelectric performance of CaMnO3-based ceramics, Journal of the European Ceramic Society, 39 (2019) 4184, DOI: 10.1016/j.jeurceramsoc.2019.06.011

[14] - W. Shin, N. Murayama, K. Ikeda, S. Sago, Thermoelectric power generation using Li-doped NiO and (Ba, Sr)PbO_3 module, J. Power Sources 103 (2001) 80, DOI: 10.1016/S0378-7753(01)00837-0.

[15] - I. Matsubara, R. Funahashi, T. Takeuchi, S. Sodeoka, T. Shimizu, Fabrication of an all-oxide thermoelectric power generator, Appl. Phys. Lett. 78 (2001) 3627, DOI: 10.1063/1.1376155.

[16] - S. Urata, R. Funahashi, T. Mihara, A. Kosuga, S. Sodeoka, T. Tanaka, Power Generation of a p-Type $Ca_3Co_4O_9$/n-Type $CaMnO_3$ Module, Int. J. Ceram. Technol. 4 (2007) 535, DOI: 10.1111/j.1744-7402.2007.02173.x.

[17] - R. Funahashi, S. Urata, Fabrication and Application of an Oxide Thermoelectric System, Int. J. Ceram. Technol. 4 (2007) 297, DOI: 10.1111/j.1744-7402.2007.02144.x.

[18] - S.F. Hayashi, T. Nakamura, K. Kageyama, H. Takagi, Monolithic Thermoelectric Devices Prepared with Multilayer Cofired Ceramics

Technology, Jpn. J. Appl. Phys. 49 (2010) 096505, DOI: 10.1143/JJAP.49.096505.

[19] - S.M. Choi, K.H. Lee, C.H. Lim, W.S. Seo, Oxide-based thermoelectric power generation module using p-type $Ca_3Co_4O_9$ and n-type $(ZnO)_7In_2O_3$ legs, Energy Convers. Manag. 52 (2011) 335-339, DOI: 10.1016/j.enconman.2010.07.005.

[20] - https://tecteg.com/wp-content/uploads/2014/09/CMO-32-62S-OXIDE-ONLY-new.pdf, last access Oct2019.

[21] - F.M. Costa, N.M. Ferreira, S. Rasekh, A.J.S. Fernandes, M.A. Torres, M.A. Madre, J.C. Diez, A.Sotelo, Very Large Superconducting Currents Induced by Growth Tailoring, Cryst. Growth Des. 15 (2015) 2094−2101, DOI: 10.1021/cg5015972.

[22] - M. A. Madre, F. M. Costa, N. M. Ferreira, S. I. R. Costa, Sh. Rasekh, M. A. Torres, J. C. Diez, V. S. Amaral, J. S. Amaral, A. Sotelo, High thermoelectric performance in Bi2-xPbxBa2Co2Ox promoted by directional growth and annealing, Journal of the European Ceramic Society 36 (2016) 67-74, DOI: 10.1016/j.jeurceramsoc.2015.09.034.

[23] - A. Sotelo, M. A. Torres, Sh. Rasekh, M. A. Madre, J. C. Diez, Effect of precursors on the microstructure and electrical properties of Bi2Ba2Co2Ox, Journal of the Australian Ceramic Society 53 (2017) 583-590, DOI: 10.1007/s41779-017-0070-6.

[24] - N.M. Ferreira, F.M. Costa, A.V. Kovalevsky, M.A. Madre, M.A. Torres, J.C. Diez, A. Sotelo, New environmentally friendly Ba-Fe-O thermoelectric material by flexible laser floating zone processing, Scripta Materialia 145 (2018) 54–57, DOI:10.1016/j.scriptamat.2017.10.011.

[25] - Rogers Germany GmbH, last access Sep2019: www.rogerscorp.com/pes.

[26] - E Yazdanshenas, A Rezania, M Karami Rad, L Rosendahl, Electrical response of thermoelectric generator to geometry variation under transient thermal boundary condition, Journal of Renewable and Sustainable Energy 10 (2018) 064705, DOI: 10.1063/1.5040166.

[27] – S.A. Atouei, A.A. Ranjbar, A. Rezania, Experimental investigation of two-stage thermoelectric generator system integrated with phase change materials, Applied Energy 208 (2017) 332-343, DOI: 10.1016/j.apenergy.2017.10.032.

[28] - S. Mahmoudinezhad, A. Rezania, A.A. Ranjbar, L.A. Rosendahl, Transient behavior of the thermoelectric generators to the load change: An experimental investigation, Energy Procedia 147 (2018) 537-543, DOI: 10.1016/j.egypro.2018.07.068.

[29] - N. M. Ferreira, A. Kovalevsky, M. A. Valente, F. M. Costa, and J. Frade, Magnetite/Hematite Core/Shell Fibres Grown by Laser Floating Zone

Method, Appl. Surf. Sci., 278 (2013) 203–206, DOI: 10.1016/j.apsusc.2013.01.108.

[30] - D. Flahaut, T. Mihara, R. Funahashi, N. Nabeshima, K. Lee, H. Ohta, K. Koumoto, Thermoelectrical properties of A-site substituted Ca1-xRexMnO3 system, J. Appl. Phys. 100 (2006) 084911.

[31] M. Mouyane, B. Itaalit, Flash Combustion Synthesis of electron doped-CaMnO3 thermoelectric oxides, Powder Technol. 264 (2014) 71-77.

[32] - Y. C. Zhou, C. L. Wang, W. B. Su, J. Liu, H. C. Wang, J. C. Li, Y. Li, J. Z. Zhai, Y. C. Zhang, L. M. Mei, Electrical properties of Dy3+/Na+ Co-doped oxide thermoelectric [Ca1-x(Na1/2Dy1/2)x]MnO3 ceramics, J. Alloys Compds. 680 (2016) 129-132. DOI: 10.1016/j.jallcom.2016.04.158.

[33] - A. Klyndyuk, E. Chizhova, N. Krasutskaya, Thermoelectric Ceramics Based on the Layered Cobaltates of Bismuth and Alkaline-Earth Metals, Universal Journal of Materials Science 5 (2017) 88-94, DOI: 10.13189/ujms.2017.050402.

[34] J.W. Seo, G.H. Kim, S.M. Choi, K. Park, High-temperature thermoelectric properties of polycrystalline CaMn1-xNbxO3-δCeramics International 44 (2018) 9204-9214, DOI: 10.1016/j.ceramint.2018.02.130

[35] L. Bocher, M. H. Aguirre, D. Logvinovich, A. Shkabko, R. Robert, M. Trottmann, and A. Weidenkaff, CaMn1-x NbxO3 (x e 0.08) Perovskite-Type Phases As Promising New High-Temperature n-Type Thermoelectric MaterialsInorg. Chem. 47 (2008) 8077-8085, DOI: 10.1021/ic800463s

[36] - C. Ni, J. T. S. Irvine, Calcium manganite as oxygen electrode materials for reversible solid oxide fuel cell, Faraday Discuss. 182 (2015) 289-305, DOI: 10.1039/c5fd00026b.

[37] - M. Mori**,** Y. Hiei, N. M. Sammes, G. A. Tompsett, Thermal-Expansion Behaviors and Mechanisms for Ca- or Sr-DopedLanthanum Manganite Perovskites under Oxidizing Atmospheres, Journal of The Electrochemical Society147 (2000) 1295-1302.

[38] - G.M. Zhao, M. B. Hunt, H. Keller, Strong Oxygen-Mass Dependence of the Thermal-Expansion Coefficientin the Manganitess (La1-xCax)d1-yMn1-yO3, Physical Review Letters 78 (1997) 995-998.

[39] - VV Kharton, E.N. Naumovich, VY Samokhval, Formation and properties of reaction layers of cobaltite electrodes on bismuth oxide electrolytes, Solid State Ionics 99 (1997) 269-280

[40] - Z. Zhan, M. ElKabbash, Z. Li, X. Li, J. Zhang, J. Rutledge, S. Singh, C. Guo*,* Enhancing thermoelectric output power via radiative cooling with nanoporous alumina, Nano Energy 65 (2019) 104060, DOI: 10.1016/j.nanoen.2019.104060.

Declaration of interests

☒ The authors declare that they have no known competing financial interests or personal relationships that could have appeared to influence the work reported in this paper.

☐The authors declare the following financial interests/personal relationships which may be considered as potential competing interests:

No conflicts of interest to declare.